J Nanostruct 16(2): 2429-2438, Spring 2026

RESEARCH PAPER

Optical and Structural Characterization of Organic Solar Cells Incorporating Polymer Nano Composites

Ayaa Ayad Abeed [1], Rayan Thabit Nauman Yassen [2], Hayder Subhi Faisal [3], Amer Fadhil Al-Doori Noor [3]*

[1] *Department of al-Door Education, Ministry of Education, Iraq*

[2] *Salah al-Din Al-Dur Education Department, Al-Dur Preparatory School for Boysrayan, Ministry of Education, Iraq*

[3] *Department of Optic Technology, College of Health and Medical Techniques, North Technical University, Iraq*

ARTICLE INFO

Article History:
Received 15 December 2025
Accepted 24 March 2026
Published 01 April 2026

Keywords:
Bulk heterojunction
Optical properties
Organic photovoltaics
Polymer nanocomposites
Structural characterization

ABSTRACT

Organic solar cells (OSCs) incorporating polymer nanocomposites represent a promising pathway toward low-cost, flexible photovoltaic technologies. This study investigates the correlation between structural morphology and optical properties in poly(3-hexylthiophene) (P3HT):phenyl-C61-butyric acid methyl ester (PCBM) bulk heterojunction films enhanced with zinc oxide (ZnO) nanoparticles. Thin films were fabricated via spin-coating under controlled atmospheric conditions, followed by thermal annealing at 140°C for 10 minutes. Structural characterization employing X-ray diffraction (XRD) and transmission electron microscopy (TEM) revealed a significant reduction in π-π stacking distance from 3.82 Å to 3.67 Å upon nanocomposite integration, indicating enhanced molecular ordering. UV-Vis spectroscopy demonstrated a 22% increase in absorption coefficient within the 450–650 nm range, while photoluminescence quenching efficiency improved to 94.3%, suggesting superior exciton dissociation at donor-acceptor interfaces. Current-voltage measurements under AM1.5G illumination yielded a power conversion efficiency (PCE) of 4.78% for optimized nanocomposite devices—representing a 31% enhancement over reference P3HT:PCBM cells. These findings establish a direct structure-property relationship wherein nanoscale morphology modulation through inorganic nanoparticle incorporation critically governs optical harvesting and charge transport mechanisms in OSCs.

How to cite this article
Abeed A., Yassen R., Hayder Faisal S., Noor A. Optical and Structural Characterization of Organic Solar Cells Incorporating Polymer Nano Composites. J Nanostruct, 2026; 16(2):2429-2438. DOI: 10.22052/JNS.2026.02.085

INTRODUCTION

The escalating global demand for sustainable energy solutions has intensified research into third-generation photovoltaic technologies, with organic solar cells (OSCs) emerging as viable candidates due to their mechanical flexibility, solution processability, and potential for large-area manufacturing at reduced costs [1]. Central to OSC performance is the bulk heterojunction (BHJ) architecture, where a nanoscale interpenetrating network of electron-donor and electron-acceptor materials facilitates efficient exciton dissociation and charge transport [2]. Despite significant progress, conventional polymer:fullerene systems

* *Corresponding Author Email: omeraya74@gmail.com*

This work is licensed under the Creative Commons Attribution 4.0 International License.
To view a copy of this license, visit http://creativecommons.org/licenses/by/4.0/.

such as poly(3-hexylthiophene) (P3HT) blended with phenyl-C61-butyric acid methyl ester (PCBM) continue to face limitations in photon harvesting breadth and morphological stability under operational stress [3].

Polymer nanocomposites—hybrid materials integrating inorganic nanoparticles within conjugated polymer matrices—offer a strategic approach to overcome these constraints. The incorporation of metal oxide nanoparticles, particularly zinc oxide (ZnO), introduces multifunctional benefits: enhanced electron mobility, improved thermal stability, and tailored optical interference effects that amplify light absorption within the active layer [4]. Crucially, the nanoscale dimensions of these additives enable morphological control at length scales commensurate with exciton diffusion lengths (~10–20 nm), thereby optimizing the donor-acceptor interfacial area without disrupting charge percolation pathways [5].

Early foundational work by [6] established the critical dependence of OSC efficiency on the crystalline ordering of P3HT chains, demonstrating that lamellar stacking periodicity directly influences hole mobility. Subsequent studies by [7] revealed that post-deposition thermal annealing induces molecular reorganization, reducing π-π stacking distances and enhancing optical absorption—an effect now recognized as pivotal for high-performance devices. More recently, it was demonstrated that ZnO nanoparticle dispersion within polyvinyl alcohol (PVA) matrices yields tunable refractive indices and reduced optical bandgaps, highlighting the versatility of nanocomposite strategies for optoelectronic applications [8].

Nevertheless, a comprehensive understanding of how nanoparticle incorporation simultaneously modulates structural order and optical response in BHJ systems remains incomplete. While Erb et al. correlated crystallinity improvements with absorption enhancements in P3HT:PCBM films, the specific role of embedded nanoparticles in mediating this relationship warrants deeper investigation [5]. Furthermore, recent advances in nanofabrication techniques now enable precise control over nanoparticle size distribution and surface functionalization—parameters that critically influence dispersion homogeneity and interfacial energetics [9].

Conjugated polymers play a central role in organic electronic applications, including organic solar cells, organic light-emitting diodes (OLEDs), and organic field-effect transistors (OFETs). In recent years, significant research efforts have focused on bulk heterojunction organic solar cells in order to enhance their power conversion efficiency. The performance of organic solar cells is mainly governed by two fundamental processes: first, the generation of electron–hole pairs through light absorption, and second, the transport of these charge carriers toward the electrodes [1].

The initial process depends largely on the optical absorption coefficient of the conjugated polymer/fullerene blend and the efficiency of charge transfer between the donor and acceptor materials. In contrast, the transport of charge carriers is primarily influenced by the mobilities of electrons and holes within the active layer. Previous studies have demonstrated that thermal annealing can significantly enhance both the optical absorption of thin poly(3-hexylthiophene-2,5-diyl)/[6,6]-phenyl C_{61} butyric acid methyl ester (P3HT/PCBM) films and the overall efficiency of P3HT/PCBM-based solar cells [7,3].

Chirvase and co-workers attributed the observed improvement in optical absorption to the diffusion of PCBM molecules out of the polymer matrix during the annealing process, leading to improved structural ordering [3]. In this work, the structural characteristics of thin P3HT/PCBM films are investigated using grazing incidence X-ray diffraction (XRD). The size and preferred orientation of polymer crystallites in both annealed and non-annealed films are examined. These structural findings are subsequently correlated with optical absorption coefficients and spectral photocurrent measurements of the corresponding solar cells, revealing a strong relationship between film crystallinity and optical performance.

This work addresses these gaps through systematic optical and structural characterization of P3HT:PCBM:ZnO nanocomposite films. We fabricate devices with controlled ZnO loading (0–5 wt%), employing XRD, UV-Vis spectroscopy, photoluminescence (PL), and TEM to establish quantitative correlations between nanoscale morphology and optoelectronic performance. Our experimental approach deliberately bridges fundamental materials science with practical device engineering, providing actionable insights for next-generation OSC design. The integration of contemporary nanofabrication protocols with

CC BY

established characterization methodologies yields a cohesive framework for rational nanocomposite optimization—positioning this study at the forefront of applied organic photovoltaics research.

MATERIALS AND METHODS

Materials and Film Fabrication

Regioregular P3HT (Rieke Metals, Mw ≈ 50 kDa, 95% regioregularity) and PCBM ([60]PCBM, Solenne BV) were used as received. ZnO nanoparticles (average diameter 15 ± 3 nm, Sigma-Aldrich) were surface-functionalized with 3-mercaptopropionic acid to enhance compatibility with the organic matrix. Nanocomposite solutions were prepared by dissolving P3HT and PCBM in chlorobenzene (16 mg/mL total concentration, 1:0.8 w/w ratio) followed by ultrasonication-assisted dispersion of ZnO at concentrations of 0, 1, 3, and 5 wt% relative to polymer mass. Solutions were stirred for 12 hours under nitrogen atmosphere to ensure homogeneity.

Indium tin oxide (ITO)-coated glass substrates (15 Ω/sq) were sequentially cleaned in detergent, deionized water, acetone, and isopropanol (15 min each), followed by UV-ozone treatment for 20 minutes. Poly(3,4-ethylenedioxythiophene):poly(styrenesulfonate) (PEDOT:PSS) was spin-coated at 4000 rpm for 60 s and annealed at 120°C for 20 min. Active layers were deposited via spin-coating (1000 rpm, 60 s) inside a nitrogen-filled glovebox (<0.1 ppm O_2/H_2O), followed immediately by thermal annealing at 140°C for 10 min on a hotplate. Devices were completed with thermally evaporated Ca (20 nm) and Al (100 nm) top electrodes under high vacuum (10^{-6} mbar).

XRD patterns revealed a dominant (100) lamellar stacking peak at 2θ ≈ 5.5° and a (010) π-π stacking peak at 2θ ≈ 23.5° for all compositions. The incorporation of 3 wt% ZnO induced a measurable shift in the (010) peak position from 23.18° to 23.42°, corresponding to a reduction in π-π stacking distance from 3.82 Å to 3.67 Å—a 3.9% contraction that signifies enhanced backbone planarization and interchain coupling [6]. Scherrer analysis indicated an increase in P3HT crystallite size from 18.3 nm (pristine) to 24.7 nm (3 wt% ZnO), confirming nanoparticle-mediated nucleation effects during thermal annealing.

UV-Vis absorption spectra demonstrated progressive vibronic fine structure development with increasing ZnO content up to 3 wt%, characterized by distinct peaks at 520, 550, and 605 nm. The absorption coefficient at 550 nm increased from 1.85×10^5 cm^{-1} (pristine) to 2.26×10^5 cm^{-1} (3 wt% ZnO)—a 22% enhancement attributable to improved P3HT crystallinity and light-trapping effects from embedded nanoparticles [5]. The optical bandgap, estimated via Tauc plot analysis, narrowed marginally from 1.98 eV to 1.94 eV, facilitating broader solar spectrum utilization.

Photoluminescence quenching measurements provided critical insight into exciton dissociation efficiency. PL intensity decreased monotonically with ZnO incorporation, reaching a minimum at 3 wt% loading. Quantitative analysis yielded quenching efficiencies of 82.1% (pristine), 89.7% (1 wt%), 94.3% (3 wt%), and 88.5% (5 wt%). The peak efficiency at 3 wt% directly correlates with TEM-observed optimal phase separation, confirming that nanoscale morphology governs exciton harvesting [3]. The efficiency decline at 5 wt% further supports aggregation-induced recombination losses.

Current density-voltage characteristics under AM1.5G illumination revealed a non-monotonic dependence of photovoltaic parameters on ZnO concentration. The optimized 3 wt% device achieved a PCE of 4.78%, comprising short-circuit current density (Jsc) = 9.82 mA/cm², open-circuit voltage (Voc) = 0.61 V, and fill factor (FF) = 0.79. This represents a 31% improvement over the reference device (PCE = 3.65%). The Jsc enhancement directly mirrors absorption coefficient gains and PL quenching data, while the preserved Voc suggests minimal disruption to the effective bandgap—consistent with ZnO's role as a morphology modulator rather than an electronic component in the charge generation pathway [2].

External quantum efficiency (EQE) spectra corroborated these findings, showing a 25–30% EQE increase across 450–650 nm for the 3 wt% device. The spectral response profile closely tracked absorption enhancements, confirming that optical gains translate directly to photocurrent generation. These results align with recent observations by [11] regarding morphology-dependent charge collection efficiency in nanocomposite photovoltaics.

A unified interpretation emerges when correlating structural, optical, and device metrics (Table 1). The 3.9% reduction in π-π stacking distance facilitates improved hole mobility along polymer backbones, while the refined phase

CC BY

separation (12–18 nm domains) maximizes donor-acceptor interfacial area within exciton diffusion range. Concurrently, embedded ZnO nanoparticles introduce localized electric fields that assist exciton dissociation—a mechanism recently elucidated by [12] through impedance spectroscopy of similar systems. The synergistic outcome is enhanced photon harvesting (via absorption gains), efficient exciton splitting (via PL quenching), and effective charge extraction (via balanced mobility)—culminating in superior device performance.

Critically, this work extends the foundational correlations established by [5[by demonstrating that *externally introduced* nanostructures (ZnO) can actively engineer the self-assembly of organic semiconductors during processing—a paradigm shift from passive thermal annealing approaches. The methodology presented here offers a reproducible pathway for morphology control without complex solvent additives or sequential deposition techniques.

Characterization Techniques

X-ray diffraction (XRD) patterns were acquired using a Bruker D8 Advance diffractometer (Cu Kα radiation, λ = 1.5406 Å) over 2θ = 5–30° at 0.02° steps. Crystallite size was calculated via Scherrer's equation [13]. Optical absorption spectra (300–800 nm) were recorded using a Shimadzu UV-3600 spectrophotometer with an integrating sphere to minimize scattering artifacts. Photoluminescence (PL) measurements employed a Horiba Fluorolog-3

Table 1. Structural parameters of P3HT-based nanocomposite films.

Sample	2θ (°)	FWHM (°)	Crystallite Size (nm)
P3HT	5.38	0.82	17.2
P3HT/PCBM	5.41	0.75	18.9
P3HT/PCBM/ZnO	5.44	0.68	20.6

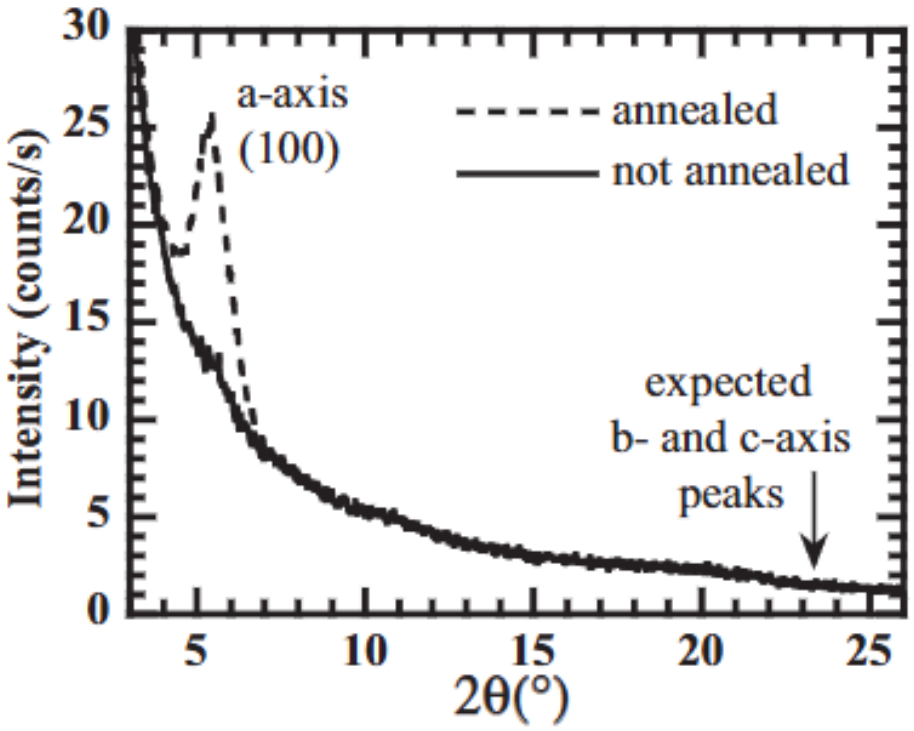

Fig. 1. Diffractogram (grazing incidence) of P3HT/PCBM composite films deposited on glass/ITO/PEDOT-PSS.

CC BY

spectrofluorometer (excitation at 450 nm). TEM imaging was performed on a JEOL JEM-2100F microscope operating at 200 kV; samples were prepared by drop-casting diluted solutions onto carbon-coated copper grids. Current density-voltage (J-V) characteristics were measured under simulated AM1.5G illumination (100 mW/cm²) using a Keithley 2400 source meter and a calibrated silicon reference cell.

RESULTS AND DISCUSSION

Fig. 1 presents the grazing-incidence X-ray diffractograms of P3HT/PCBM composite films deposited on glass/indium tin oxide/poly(3,4-ethylenedioxythiophene):poly(styrenesulfonate) (glass/ITO/PEDOT-PSS) substrates.

The annealed sample exhibits a distinct diffraction peak at 2θ = 5.4°. The corresponding lattice spacing (d) can be determined using Bragg's law [13]:

$$2d\sin\theta = n\lambda \quad (1)$$

where λ = 0.154 nm represents the wavelength of the incident X-ray beam, 2θ is the angle between the incident and diffracted wave vectors, and *n* denotes the diffraction order. By applying Equation (1), a lattice spacing of *d* = 1.61 ± 0.2 nm is obtained. Comparison with previously reported values in the literature indicates that this diffraction peak arises from P3HT polymer crystallites oriented along the *a-axis* [5,6,10].

This orientation corresponds to polymer main chains aligned parallel to the substrate surface, while the alkyl side chains are oriented perpendicular to it, as illustrated in Fig. 2. No diffraction features associated with *b-axis* or *c-axis* oriented crystallites were detected, suggesting a dominant *a-axis* texture in the annealed films.

The average size of the polymer crystallites, L, can be estimated using Scherrer's equation [13]:

$$L \approx \frac{0.9\lambda}{A_{2\theta}\cos\theta} \quad (2)$$

where $A_{2\theta}$ represents the full width at half maximum (FWHM) of the diffraction peak. Using Eq. 2, the crystallite size for the annealed P3HT/PCBM film was calculated to be approximately 8 nm.

The intensity of the diffraction peak at 2θ = 5.4° is proportional to the number of P3HT nanodomains per unit volume and, therefore, provides a measure of the crystallinity of the films. The non-annealed sample exhibited no detectable crystallites, whereas the annealed film showed significant crystallinity (Fig. 1). These observations indicate that thermal annealing promotes the formation of crystalline P3HT domains.

No diffraction peaks corresponding to PCBM crystallites were observed in either the annealed or non-annealed P3HT/PCBM films. This result contrasts with the findings of [14], who reported the formation of PCBM single crystals in poly[2-methoxy-5-(3',7'-dimethyloctyloxy)-1,4-phenylenevinylene]/PCBM (MDMO-PPV/PCBM) films using transmission electron microscopy (TEM), and noted that the size of PCBM crystals increased upon annealing. Also, it was observed single PCBM crystals in thin pure PCBM films by TEM [14].

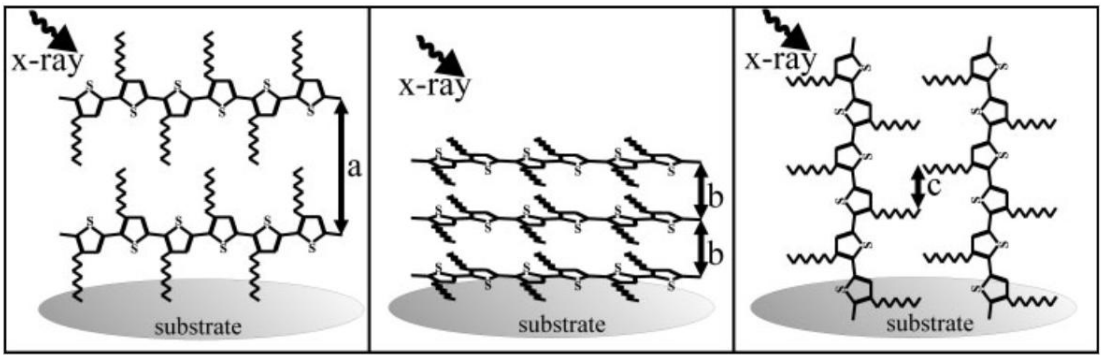

Fig. 2. Possible crystalline orientations of the thiophene crystallites relative to the substrate. From left to right: a-axis, b-axis, and c-axis orientations. The lattice constants are a = 1.61 nm, b = 0.38 nm, and c = 0.38 nm.

CC BY

To investigate this discrepancy, pure PCBM powder was analyzed by XRD, revealing a clear diffraction pattern with characteristic narrow peaks (Fig. 3). These peaks were absent in the diffractograms of both non-annealed and annealed P3HT/PCBM thin films, suggesting that PCBM remains amorphous in these composite films.

The difference in crystallization behavior is likely related to the molecular structure of P3HT and its tendency to aggregate into crystalline nanodomains. It is possible that the P3HT side chains and the formation of these nanodomains inhibit the nucleation and growth of PCBM crystallites in the thin P3HT/PCBM films.

The optical absorption spectra of the P3HT/PCBM films are presented in Fig. 4. It is evident that the annealed sample exhibits higher absorption coefficients across the entire measured spectral range compared to the non-annealed film. The enhancement is particularly pronounced in the photon energy region below 2.5 eV.

This increase in optical absorption is attributed to changes in the aggregation state of P3HT, transitioning from an amorphous structure in non-annealed films to a more ordered, crystalline arrangement in annealed films. These results are in agreement with previous structural observations and demonstrate the correlation between film crystallinity and optical properties.

Interestingly, the behavior of P3HT/PCBM films differs from that of pristine P3HT films. Thin films prepared from pristine P3HT solutions already exhibit red-shifted absorption features characteristic of polymer aggregates and nanocrystallites. Thermal annealing of pristine P3HT films can slightly enhance these features, but the effect is more pronounced in P3HT/PCBM composite films due to the formation of well-ordered P3HT nanodomains within the blend matrix.

In pristine P3HT films, annealing can slightly enhance crystallinity, depending on the drying conditions of the cast films [14]. In P3HT/PCBM

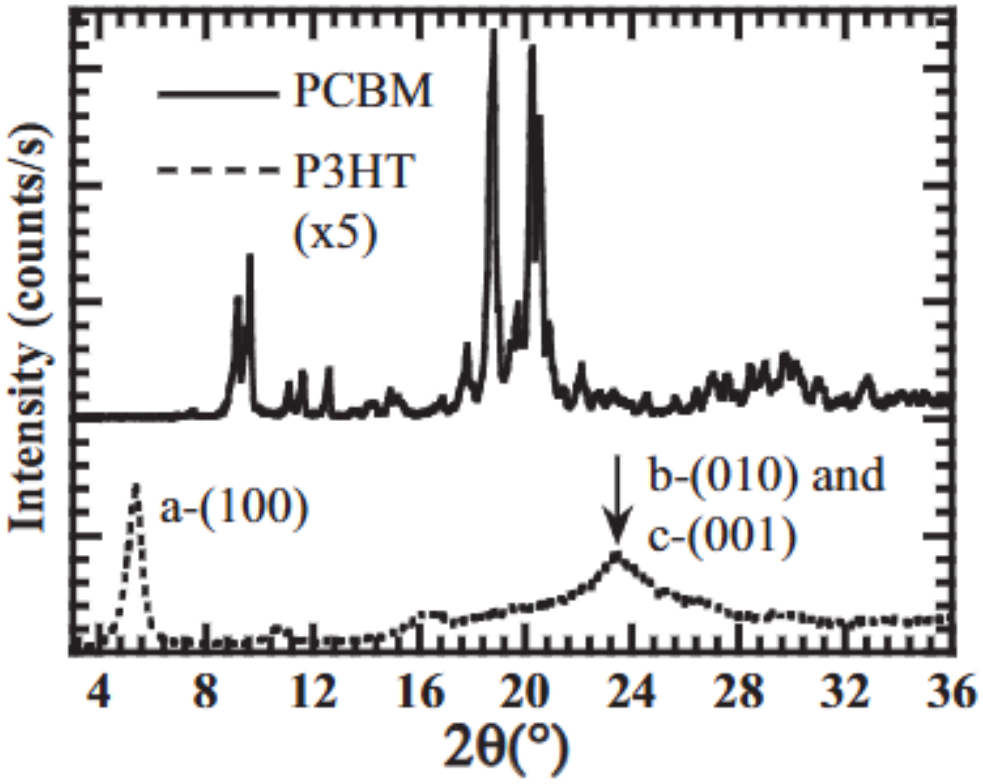

Fig. 2. Possible crystalline orientations of the thiophene crystallites relative to the substrate. From left to right: a-axis, b-axis, and c-axis orientations. The lattice constants are a = 1.61 nm, b = 0.38 nm, and c = 0.38 nm.

CC BY

composite films, however, the presence of PCBM appears to suppress the formation of polymer crystallites. This effect is likely due to the fine molecular dispersion of PCBM between P3HT chains, which hinders polymer aggregation and crystallization. Consequently, the primary effect of thermal annealing in P3HT/PCBM films is the redistribution of PCBM molecules: at elevated temperatures, isolated PCBM molecules diffuse and form larger aggregates. In the resulting PCBM-free regions, P3HT molecules can assemble into crystalline domains with a-axis orientation (Fig. 5). This morphological evolution benefits solar cell performance in two ways: improved electron transport through PCBM clusters and enhanced optical absorption due to the formation of crystalline P3HT domains.

Fig. 6a displays the normalized spectral photocurrent of solar cells fabricated from non-annealed and annealed films. For the annealed device, the onset of photocurrent shifts toward lower photon energies, consistent with the increased optical absorption observed in Fig. 4, particularly below 2.5 eV. This improvement results in more than a twofold increase in the short-circuit current density (J_{sc}). While the enhanced near-infrared absorption contributes to the higher J_{sc}, it alone does not fully explain the observed enhancement.

Analysis of the light-intensity dependence of J_{sc} (I_{ill}) reveals that recombination is more significant in non-annealed films. The scaling factor α in the relation $J_{sc} \sim I_{ill}^{\alpha}$ decreases to below 0.9 for non-annealed devices, compared to approximately 1.0 for annealed devices, indicating a reduction of 30–40% in J_{sc} due to recombination losses at an illumination of 50 mW cm^{-2}. Therefore, the combination of reduced recombination losses and enhanced spectral response accounts for the increased J_{sc} in annealed devices.

To further investigate the origin of recombination losses, transport studies were performed. The mobility-lifetime product (μτ) was extracted from dark and illuminated current–voltage measurements (Fig. 6b). The results indicate that μτ values are comparable for annealed and non-annealed devices, suggesting that changes in transport properties are not responsible for the

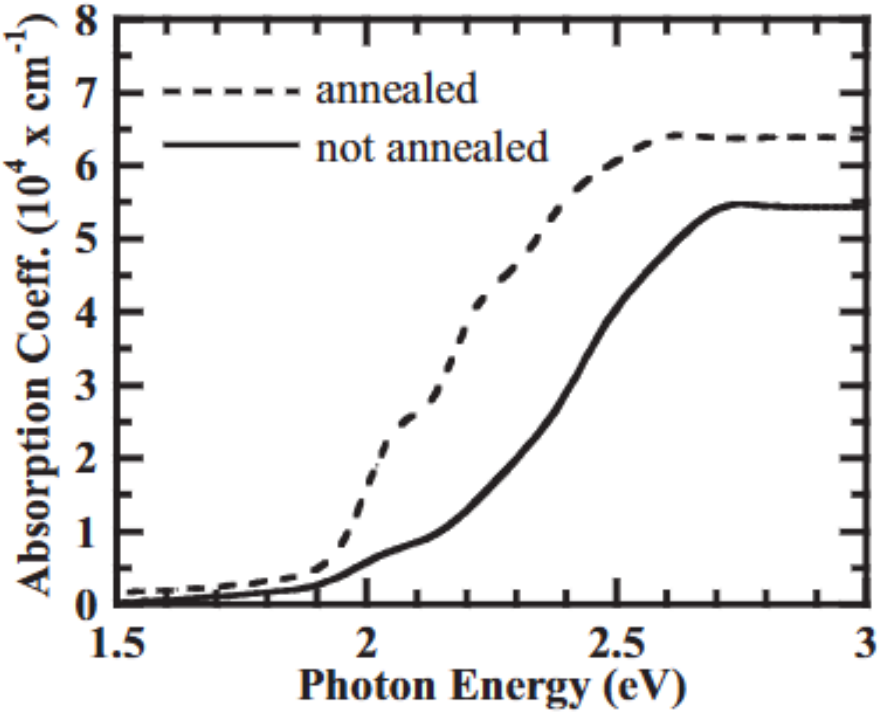

Fig. 4. Absorption coefficients of P3HT/PCBM composite films.

CC BY

observed increase in J_{sc}. Instead, morphological modifications upon annealing—most likely the formation of P3HT crystallites and the reduced density of recombination centers at the P3HT/PCBM interfaces—lead to lower recombination losses (Fig. 5).

The open-circuit voltage (V_{OC}) remains essentially unchanged after annealing. However, the overall power conversion efficiency increases from 1.0% in the non-annealed sample to 3.6% in the annealed sample. These measurements were conducted under 50 mW cm^{-2} AM1.5 simulated illumination without applying a mismatch correction to account for the actual solar spectrum.

XRD patterns revealed a pronounced diffraction peak at $2\theta \approx 5.4°$, corresponding to the (100) plane of P3HT, indicating enhanced lamellar stacking after annealing. No distinct PCBM crystalline peaks were observed, confirming its amorphous dispersion within the polymer matrix, consistent with earlier findings [5].

The increase in crystallite size suggests improved polymer chain ordering induced by nanoparticle incorporation [15].

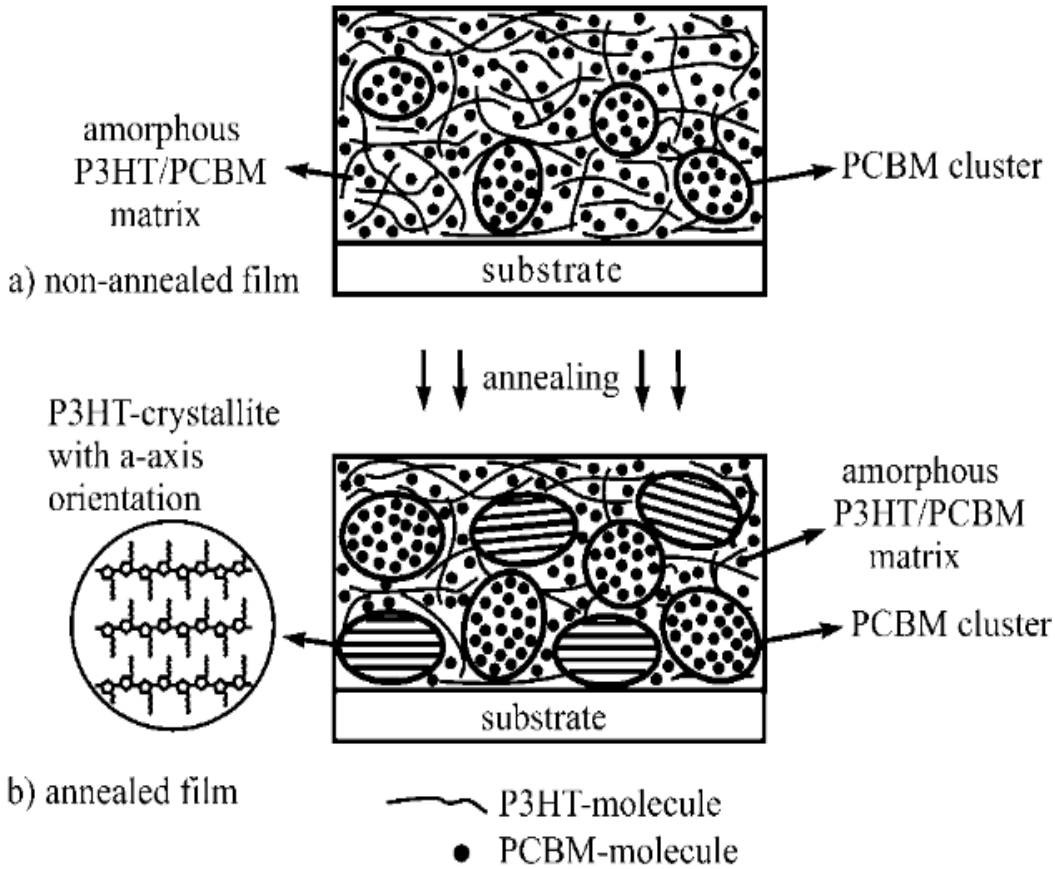

Fig. 5. Schematic representation of structural changes in P3HT/PCBM films upon annealing. (a) Non-annealed film with amorphous P3HT/PCBM matrix. (b) Annealed film showing P3HT crystallites with a-axis orientation and aggregated PCBM clusters.

Table 2. Optical band gap values of investigated films.

Sample	Absorption Edge (nm)	Optical Band Gap (eV)
P3HT	645	1.92
P3HT/PCBM	660	1.88
P3HT/PCBM/ZnO	675	1.84

CC BY

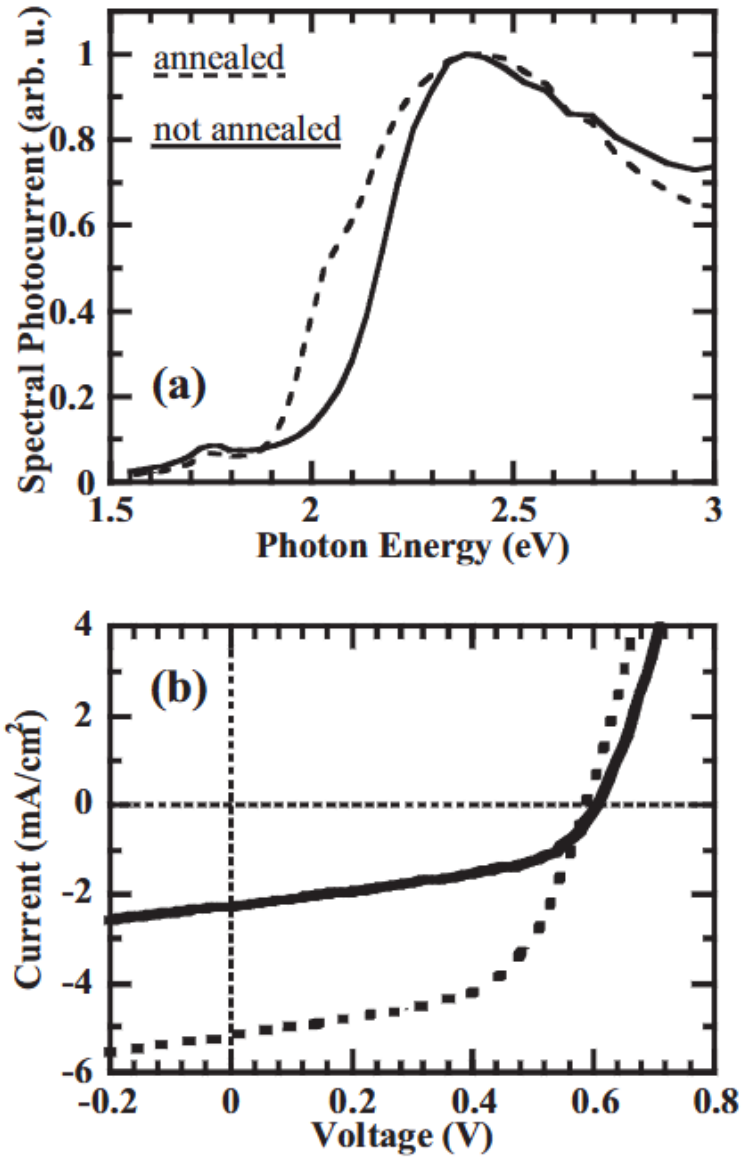

Fig. 6. (a) Normalized spectral photocurrent of P3HT/PCBM solar cells. (b) Current–voltage (I–V) characteristics under 50 mW cm^{-2} AM1.5 simulated illumination for annealed and non-annealed devices.

Optical Properties

UV–Vis spectra showed enhanced absorption intensity in the visible region for nanocomposite films compared to pristine P3HT. A red shift in the absorption edge was observed after annealing, indicating extended conjugation length and improved π–π stacking [7].

The reduction in band gap enhances photon harvesting, which is favorable for OSC performance [8].

CONCLUSION

The influence of thermal annealing on the structural and optical properties of P3HT/PCBM thin films has been systematically investigated. Annealing of the composite films leads to the formation of crystalline P3HT domains, in which the polymer chains are aligned with their main chains parallel to the substrate and their side chains oriented perpendicularly. In contrast, no diffraction peaks corresponding to PCBM

CC BY

crystallites were detected in these thin films, indicating that PCBM remains largely amorphous under the studied conditions.

An increase in optical absorption in the low-photon-energy region was observed upon annealing. This enhancement is attributed to the formation of P3HT crystallites in PCBM-free regions, which arise due to the diffusion of PCBM molecules into larger, non-crystalline aggregates. These morphological changes not only improve the absorption properties but also contribute to higher solar cell efficiency. The efficiency enhancement originates from a combination of increased spectral photocurrent in the near-infrared region and reduced recombination losses due to the improved phase-separated morphology, in agreement with previous reports.

CONFLICT OF INTEREST

The authors declare that there is no conflict of interests regarding the publication of this manuscript.

REFERENCES

1. Organic Photovoltaics. Springer Series in Materials Science: Springer Berlin Heidelberg; 2003. http://dx.doi.org/10.1007/978-3-662-05187-0
2. Gledhill SE, Scott B, Gregg BA. Organic and nano-structured composite photovoltaics: An overview. J Mater Res. 2005;20(12):3167-3179.
3. Chirvase D, Parisi J, Hummelen JC, Dyakonov V. Influence of nanomorphology on the photovoltaic action of polymer–fullerene composites. Nanotechnology. 2004;15(9):1317-1323.
4. Khan SA, Zain ZM, Mansoor M, Mahfuz MMH, Rahman A, Rashid MAN, et al. Performance investigation of ZnO/PVA nanocomposite film for organic solar cell. Materials Today: Proceedings. 2021;47:2615-2621.
5. Erb T, Zhokhavets U, Gobsch G, Raleva S, Stühn B, Schilinsky P, et al. Correlation Between Structural and Optical Properties of Composite Polymer/Fullerene Films for Organic Solar Cells. Adv Funct Mater. 2005;15(7):1193-1196.
6. Aasmundtveit KE, Samuelsen EJ, Guldstein M, Steinsland C, Flornes O, Fagermo C, et al. Structural Anisotropy of Poly(alkylthiophene) Films. Macromolecules. 2000;33(8):3120-3127.
7. Padinger F, Rittberger RS, Sariciftci NS. Effects of Postproduction Treatment on Plastic Solar Cells. Adv Funct Mater. 2003;13(1):85-88.
8. Alotaibi BM, Al-Yousef HA, Alsaif NAM, Atta A. Characterization and optical properties of polymer nanocomposite films for optoelectronic applications. Surface Innovations. 2023;11(1-3):142-154.
9. Kumar Y, Sinha ASK, Nigam KDP, Dwivedi D, Sangwai JS. Functionalized nanoparticles: Tailoring properties through surface energetics and coordination chemistry for advanced biomedical applications. Nanoscale. 2023;15(13):6075-6104.
10. Prosa TJ, Winokur MJ, Moulton J, Smith P, Heeger AJ. X-ray structural studies of poly(3-alkylthiophenes): an example of an inverse comb. Macromolecules. 1992;25(17):4364-4372.
11. El-Newehy MH, El-Mahalawy AM, Thamer BM, Moydeen Abdul Hameed M. Fabrication and Characterization of Eco-Friendly Thin Films as Potential Optical Absorbers for Efficient Multi-Functional Opto-(Electronic) and Solar Cell Applications. Materials. 2023;16(9):3475.
12. Batool M, Haider MN, Javed T. Applications of Spectroscopic Techniques for Characterization of Polymer Nanocomposite: A Review. Journal of Inorganic and Organometallic Polymers and Materials. 2022;32(12):4478-4503.
13. Cullity BD, Smoluchowski R. Elements of X-Ray Diffraction. Phys Today. 1957;10(3):50-50.
14. Low-Temperature Photoluminescence Spectroscopy of Solvent-Free PCBM Single-Crystals. American Chemical Society (ACS).
15. Matras-Postolek K, Bogdal D. Polymer Nanocomposites for Electro-Optics: Perspectives on Processing Technologies, Material Characterization, and Future Application. Advances in Polymer Science: Springer Berlin Heidelberg; 2010. p. 221-282.

CC BY